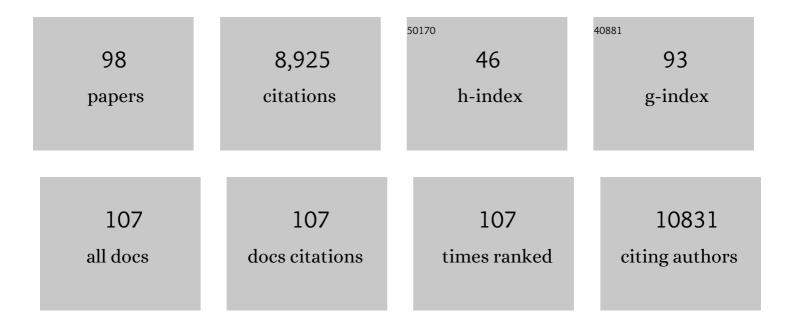
List of Publications by Year in descending order

Source: https://exaly.com/author-pdf/3598481/publications.pdf Version: 2024-02-01



#	Article	IF	CITATIONS
1	New electrolyzer principles: decoupled water splitting. , 2022, , 407-454.		4
2	Magnon transport in the presence of antisymmetric exchange in a weak antiferromagnet. Journal of Magnetism and Magnetic Materials, 2022, 543, 168631.	1.0	1
3	Carbon-cloth-supported nickel hydroxide anodes for electrochemical–thermally-activated chemical (E-TAC) water splitting. Journal of Materials Chemistry A, 2022, 10, 726-739.	5.2	9
4	Considerations for the Accurate Measurement of Incident Photon to Current Efficiency in Photoelectrochemical Cells. Frontiers in Energy Research, 2022, 9, .	1.2	6
5	Electronic excitations of 뱉^Fe2O3 heteroepitaxial films measured by resonant inelastic x-ray scattering at the Fe L edge. Physical Review B, 2022, 105, .	1.1	2
6	External Quantum Efficiency Spectra of BiVO ₄ Thin Film Photoanodes under Bias Illumination. Journal of the Electrochemical Society, 2022, 169, 046513.	1.3	1
7	Parallel water photo-oxidation reaction pathways in hematite photoanodes: implications for solar fuel production. Energy and Environmental Science, 2022, 15, 2445-2459.	15.6	9
8	High Performance Core/Shell Ni/Ni(OH) ₂ Electrospun Nanofiber Anodes for Decoupled Water Splitting. Advanced Functional Materials, 2021, 31, 2008118.	7.8	32
9	Extraction of mobile charge carrier photogeneration yield spectrum of ultrathin-film metal oxide photoanodes for solar water splitting. Nature Materials, 2021, 20, 833-840.	13.3	32
10	Wasted photons: photogeneration yield and charge carrier collection efficiency of hematite photoanodes for photoelectrochemical water splitting. Energy and Environmental Science, 2021, 14, 4584-4598.	15.6	22
11	Effect of Doping and Excitation Wavelength on Charge Carrier Dynamics in Hematite by Timeâ€Resolved Microwave and Terahertz Photoconductivity. Advanced Functional Materials, 2020, 30, 1901590.	7.8	25
12	Decoupled Photoelectrochemical Water Splitting System for Centralized Hydrogen Production. Joule, 2020, 4, 448-471.	11.7	91
13	Defect Segregation and Its Effect on the Photoelectrochemical Properties of Ti-Doped Hematite Photoanodes for Solar Water Splitting. Chemistry of Materials, 2020, 32, 1031-1040.	3.2	23
14	Propagation Length of Antiferromagnetic Magnons Governed by Domain Configurations. Nano Letters, 2020, 20, 306-313.	4.5	48
15	The mechanism of grain growth at general grain boundaries in SrTiO3. Scripta Materialia, 2020, 188, 206-211.	2.6	13
16	Structural sensitivity of the spin Hall magnetoresistance in antiferromagnetic thin films. Physical Review B, 2020, 102, .	1.1	19
17	Operando X-ray Absorption Spectroscopy (XAS) Observation of Photoinduced Oxidation in FeNi (Oxy)hydroxide Overlayers on Hematite (1±-Fe ₂ O ₃) Photoanodes for Solar Water Splitting. Langmuir, 2020, 36, 11564-11572.	1.6	9
18	An insulating doped antiferromagnet with low magnetic symmetry as a room temperature spin conduit. Applied Physics Letters, 2020, 117, .	1.5	12

AVNER ROTHSCHILD

#	Article	IF	CITATIONS
19	Transpiration Driven Electrokinetic Power Generator. ACS Nano, 2019, 13, 12703-12709.	7.3	134
20	Decoupled hydrogen and oxygen evolution by a two-step electrochemical–chemical cycle for efficient overall water splitting. Nature Energy, 2019, 4, 786-795.	19.8	296
21	Empirical Analysis of the Photoelectrochemical Impedance Response of Hematite Photoanodes for Water Photo-oxidation. Journal of Physical Chemistry Letters, 2018, 9, 1466-1472.	2.1	19
22	Different Roles of Fe _{1–<i>x</i>} Ni _{<i>x</i>} OOH Cocatalyst on Hematite (α-Fe ₂ O ₃) Photoanodes with Different Dopants. ACS Catalysis, 2018, 8, 2754-2759.	5.5	53
23	The "Rust―Challenge: On the Correlations between Electronic Structure, Excited State Dynamics, and Photoelectrochemical Performance of Hematite Photoanodes for Solar Water Splitting. Advanced Materials, 2018, 30, e1706577.	11.1	83
24	The Spatial Collection Efficiency of Charge Carriers in Photovoltaic and Photoelectrochemical Cells. Joule, 2018, 2, 210-224.	11.7	36
25	Implementing Strong Interference in Ultrathin Film Top Absorbers for Tandem Solar Cells. ACS Photonics, 2018, 5, 5068-5078.	3.2	19
26	Two-site H2O2 photo-oxidation on haematite photoanodes. Nature Communications, 2018, 9, 4060.	5.8	22
27	Film Flip and Transfer Process to Enhance Light Harvesting in Ultrathin Absorber Films on Specular Backâ€Reflectors. Advanced Materials, 2018, 30, 1802781.	11.1	12
28	Live cyanobacteria produce photocurrent and hydrogen using both the respiratory and photosynthetic systems. Nature Communications, 2018, 9, 2168.	5.8	104
29	Influence of Ti Doping Levels on the Photoelectrochemical Properties of Thin-Film Hematite (α-Fe ₂ O ₃) Photoanodes. Journal of Physical Chemistry C, 2017, 121, 4206-4213.	1.5	51
30	Photoelectrochemical water splitting in separate oxygen and hydrogen cells. Nature Materials, 2017, 16, 646-651.	13.3	418
31	Beating the Efficiency of Photovoltaics-Powered Electrolysis with Tandem Cell Photoelectrolysis. ACS Energy Letters, 2017, 2, 45-51.	8.8	73
32	Magnetic states at the surface of <mml:math xmlns:mml="http://www.w3.org/1998/Math/MathML"><mml:mrow><mml:mi>α</mml:mi><mml:mtext>â^'mathvariant="normal">O<mml:mn>3</mml:mn></mml:mtext></mml:mrow> thin films doped with Ti, Zn, or Sn. Physical Review B, 2017, 96, .</mml:math 	ml:mtext> 1.1	<mml:msub><</mml:msub>
33	Negative differential resistance and hysteresis in Au/MoO _{3â^î^} /Au devices. RSC Advances, 2017, 7, 38059-38068.	1.7	12
34	Wavelength Dependent Photocurrent of Hematite Photoanodes: Reassessing the Hole Collection Length. Journal of Physical Chemistry C, 2017, 121, 28287-28292.	1.5	15
35	Accurate determination of the charge transfer efficiency of photoanodes for solar water splitting. Physical Chemistry Chemical Physics, 2017, 19, 20383-20392.	1.3	49
	Oxygen transport in epitaxia		

36 SrTiO<sub>3</sub>/SrTi<sub>1 â^' <i>x</i></sub>Fe<sub><i>x</sub>
multilayer stacks. Journal of Sensors and Sensor Systems, 2017, 6, 107-119.

#	Article	IF	CITATIONS
37	(Invited) Reflections on Rust: Iron Oxide Photoelectrodes for Solar Energy Conversion and Storage. ECS Meeting Abstracts, 2017, , .	0.0	0
38	Nano Gold Rush: On the Origin of the Photocurrent Enhancement in Hematite Photoanodes Decorated with Gold Nanoparticles. Journal of Physical Chemistry C, 2016, 120, 15042-15051.	1.5	15
39	Effect of Orientation on Bulk and Surface Properties of Sn-doped Hematite (α-Fe ₂ O ₃) Heteroepitaxial Thin Film Photoanodes. Journal of Physical Chemistry C, 2016, 120, 28961-28970.	1.5	35
40	High Solar Flux Concentration Water Splitting with Hematite (αâ€Fe ₂ O ₃) Photoanodes. Advanced Energy Materials, 2016, 6, 1500817.	10.2	72
41	Empirical in operando analysis of the charge carrier dynamics in hematite photoanodes by PEIS, IMPS and IMVS. Physical Chemistry Chemical Physics, 2016, 18, 23438-23457.	1.3	131
42	Heterogeneous Doping to Improve the Performance of Thin-Film Hematite Photoanodes for Solar Water Splitting. ACS Energy Letters, 2016, 1, 827-833.	8.8	59
43	Hybrid bio-photo-electro-chemical cells for solar water splitting. Nature Communications, 2016, 7, 12552.	5.8	74
44	Rigorous substrate cleaning process for reproducible thin film hematite (α-Fe ₂ O ₃) photoanodes. Journal of Materials Research, 2016, 31, 1565-1573.	1.2	28
45	Parallel Band and Hopping Electron Transport in SrTiO ₃ . Advanced Electronic Materials, 2016, 2, 1500368.	2.6	8
46	Heteroepitaxial hematite photoanodes as a model system for solar water splitting. Journal of Materials Chemistry A, 2016, 4, 3052-3060.	5.2	30
47	Systematic comparison of different dopants in thin film hematite (α-Fe ₂ O ₃) photoanodes for solar water splitting. Journal of Materials Chemistry A, 2016, 4, 3091-3099.	5.2	112
48	High Temperature Electrolysis of CO ₂ for Fuel Production. Journal of the Electrochemical Society, 2016, 163, F79-F87.	1.3	13
49	Separation of light confinement and absorption sites for enhancing solar water splitting. Journal of Materials Chemistry A, 2016, 4, 3043-3051.	5.2	4
50	Schottky barrier height switching in thin metal oxide films studied in diode and solar cell device configurations. Journal of Applied Physics, 2015, 118, .	1.1	6
51	Fibrous TiO2 gas sensors produced by electrospinning. Journal of Electroceramics, 2015, 35, 148-159.	0.8	16
52	The Photosystem II D1-K238E mutation enhances electrical current production using cyanobacterial thylakoid membranes in a bio-photoelectrochemical cell. Photosynthesis Research, 2015, 126, 161-169.	1.6	23
53	Photosynthetic Membranes of Synechocystis or Plants Convert Sunlight to Photocurrent through Different Pathways due to Different Architectures. PLoS ONE, 2015, 10, e0122616.	1.1	26
54	Thin-walled SnO ₂ nanotubes functionalized with Pt and Au catalysts via the protein templating route and their selective detection of acetone and hydrogen sulfide molecules. Nanoscale, 2015, 7, 16417-16426.	2.8	144

#	Article	IF	CITATIONS
55	In-situ high resolution transmission electron microscopy observation of silicon nanocrystal nucleation in a SiO2 bilayered matrix. Applied Physics Letters, 2014, 105, 053116.	1.5	9
56	Selective Detection of Acetone and Hydrogen Sulfide for the Diagnosis of Diabetes and Halitosis Using SnO ₂ Nanofibers Functionalized with Reduced Graphene Oxide Nanosheets. ACS Applied Materials & Interfaces, 2014, 6, 2588-2597.	4.0	347
57	On the Solar to Hydrogen Conversion Efficiency of Photoelectrodes for Water Splitting. Journal of Physical Chemistry Letters, 2014, 5, 3330-3334.	2.1	128
58	Selectivity enhancement of SnO2 nanofiber gas sensors by functionalization with Pt nanocatalysts and manipulation of the operation temperature. Sensors and Actuators B: Chemical, 2013, 188, 156-168.	4.0	95
59	Memory diodes with nonzero crossing. Applied Physics Letters, 2013, 102, .	1.5	23
60	Resonant light trapping in ultrathin films for water splitting. Nature Materials, 2013, 12, 158-164.	13.3	309
61	Defect chemical modeling of Pd/ZnO Schottky junctions. Solid State Ionics, 2013, 233, 80-86.	1.3	2
62	Advances and new directions in gas-sensing devices. Acta Materialia, 2013, 61, 974-1000.	3.8	282
63	Identifying champion nanostructures for solar water-splitting. Nature Materials, 2013, 12, 842-849.	13.3	527
64	Epitaxial growth of Nb-doped SrTiO3 films by pulsed laser deposition. Applied Surface Science, 2012, 258, 9496-9500.	3.1	10
65	Microstructure evolution of TiO2 gas sensors produced by electrospinning. Sensors and Actuators B: Chemical, 2012, 171-172, 118-126.	4.0	29
66	Enhancement in the Performance of Ultrathin Hematite Photoanode for Water Splitting by an Oxide Underlayer. Advanced Materials, 2012, 24, 2699-2702.	11.1	271
67	Thermally oxidized iron oxide nanoarchitectures for hydrogen production by solar-induced water splitting. International Journal of Hydrogen Energy, 2012, 37, 8102-8109.	3.8	54
68	Probing the photoelectrochemical properties of hematite (α-Fe ₂ O ₃) electrodes using hydrogen peroxide as a hole scavenger. Energy and Environmental Science, 2011, 4, 958-964.	15.6	933
69	Nanostructured metal oxide gas sensors prepared by electrospinning. Polymers for Advanced Technologies, 2011, 22, 318-325.	1.6	120
70	Resolving Bulk and Grain Boundary Transport Properties of TiO ₂ Thin Films Enabled by Laserâ€Induced Anisotropic Morphology. Advanced Materials, 2011, 23, 3266-3271.	11.1	5
71	Ultrasensitive and Highly Selective Gas Sensors Based on Electrospun SnO ₂ Nanofibers Modified by Pd Loading. Advanced Functional Materials, 2010, 20, 4258-4264.	7.8	368
72	Tunable gas sensing properties of p- and n-doped ZnO thin films. Sensors and Actuators B: Chemical, 2010, 148, 379-387.	4.0	29

#	Article	IF	CITATIONS
73	In situ sonochemical hydrolysis and deposition of composite layers of ionic liquid entrapped in colloidal silica network and their application as sensors for various gases. Ultrasonics Sonochemistry, 2010, 17, 726-729.	3.8	5
74	Defect chemistry of <mml:math <br="" xmlns:mml="http://www.w3.org/1998/Math/MathML">display="inline"><mml:mrow><mml:mi>p</mml:mi><mml:mi>n</mml:mi></mml:mrow></mml:math> junctions in complex oxides. Physical Review B, 2010, 82, .	1.1	17
75	Highly enhanced electrochemical performance of silicon-free platinum–yttria stabilized zirconia interfaces. Journal of Electroceramics, 2009, 22, 428-435.	0.8	45
76	Hollow ZnO Nanofibers Fabricated Using Electrospun Polymer Templates and Their Electronic Transport Properties. ACS Nano, 2009, 3, 2623-2631.	7.3	208
77	Processing-Microstructure-Properties Correlation of Ultrasensitive Gas Sensors Produced by Electrospinning. Chemistry of Materials, 2009, 21, 9-11.	3.2	98
78	Fabrication and gas sensing properties of hollow SnO2 hemispheres. Chemical Communications, 2009, , 4019.	2.2	85
79	Macroporous TiO2 thin film gas sensors obtained using colloidal templates. Sensors and Actuators B: Chemical, 2008, 130, 9-13.	4.0	61
80	Electrospun nanostructured TiO <inf>2</inf> gas sensors. , 2008, , .		1
81	Tailoring the gas sensing properties of ZnO thin films through oxygen nonstoichiometry. Applied Physics Letters, 2008, 93, .	1.5	28
82	Titanium oxide thin film gas sensors. Physica Scripta, 2007, T129, 157-159.	1.2	10
83	Electronic Structure, Defect Chemistry, and Transport Properties of SrTi1-xFexO3-ySolid Solutions. Chemistry of Materials, 2006, 18, 3651-3659.	3.2	220
84	Microsphere Templating as Means of Enhancing Surface Activity and Gas Sensitivity of CaCu3Ti4O12Thin Films. Nano Letters, 2006, 6, 193-198.	4.5	147
85	Ultrasensitive Chemiresistors Based on Electrospun TiO2 Nanofibers. Nano Letters, 2006, 6, 2009-2013.	4.5	573
86	Gas sensors: New materials and processing approaches. Journal of Electroceramics, 2006, 17, 1005-1012.	0.8	52
87	Direct current bias effects on grain boundary Schottky barriers in CaCu3Ti4O12. Applied Physics Letters, 2006, 88, 072902.	1.5	60
88	Temperature-independent resistive oxygen sensors based on SrTi1â^'xFexO3â^'δ solid solutions. Sensors and Actuators B: Chemical, 2005, 108, 223-230.	4.0	102
89	The electrical properties and stability of SrTi0.65Fe0.35O3â ^{~1} δ thin films for automotive oxygen sensor applications. Sensors and Actuators B: Chemical, 2005, 108, 231-237.	4.0	59
90	On the Relationship Between the Grain Size and Gas-Sensitivity of Chemo-Resistive Metal-Oxide Gas Sensors with Nanosized Grains. Journal of Electroceramics, 2004, 13, 697-701.	0.8	56

AVNER ROTHSCHILD

#	Article	IF	CITATIONS
91	The effect of grain size on the sensitivity of nanocrystalline metal-oxide gas sensors. Journal of Applied Physics, 2004, 95, 6374-6380.	1.1	560
92	Surface photovoltage spectroscopy study of reduced and oxidized nanocrystalline TiO2 films. Surface Science, 2003, 532-535, 456-460.	0.8	56
93	Numerical computation of chemisorption isotherms for device modeling of semiconductor gas sensors. Sensors and Actuators B: Chemical, 2003, 93, 362-369.	4.0	73
94	Electronic and transport properties of reduced and oxidized nanocrystalline TiO2 films. Applied Physics Letters, 2003, 82, 574-576.	1.5	64
95	Quantitative evaluation of chemisorption processes on semiconductors. Journal of Applied Physics, 2002, 92, 7090-7097.	1.1	64
96	Title is missing!. Journal of Materials Science, 2001, 9, 157-162.	1.2	8
97	Low Temperature Reoxidation Mechanism in Nanocrystalline TiO[sub 2â^î] Thin Films. Journal of the Electrochemical Society, 2001, 148, H85.	1.3	14
98	Sensing behavior of TiO2 thin films exposed to air at low temperatures. Sensors and Actuators B: Chemical, 2000, 67, 282-289.	4.0	138